Determining the Mass and Spin of the Black Hole in GRB 220101A Using 0.1-100 GeV Data Observed by Fermi/LAT

S. Sheykhi, S. Noroozi

Department of Fundamental Physics, Faculty of Physics, Alzahra University, Tehran, Iran

F. Rastgarnia

ICRANet, Piazza della Repubblica 10, I-65122 Pescara, Italy
ICRA, Dipartimento di Fisica, Università di Roma "La Sapienza", Piazzale Aldo Moro 5, I-00185 Roma, Italy E-mail: fatemeh.rastegarnia@icranet.org

R. Moradi

Key Laboratory of Particle Astrophysics, Institute of High Energy Physics, Chinese Academy of Sciences, Beijing 100049, People's Republic of China E-mail: rmoradi@ihep.ac.cn

GRB 220101A, detected by the Swift satellite with a redshift of (z = 4.618) and an equivalent isotropic energy of 4×10^{54} ergs, is categorized as a Binary Driven Hypernova of type one (BdHN I). Within the BdHN model, the GeV emission observed by Fermi/LAT is attributed to the newborn Kerr black hole. By analyzing this emission, we determine the mass and spin of the Kerr black hole. The theoretical values obtained for the mass are consistent with those expected for black holes in the literature, supporting the hypothesis that the GeV radiation is indeed powered by the newborn Kerr black hole.

Keywords: Gamma-ray burst; GeV emission; Black hole; Neutron star.

1. Introduction

The Binary Driven Hypernova (BdHN) model suggests that the progenitors of long gamma-ray bursts (GRBs) are binary systems comprising a carbon-oxygen (CO) star and a neutron star (NS)[1–6]. In this scenario, a supernova (SN) explosion results in the formation of a newborn neutron star (νNS). For BdHN type I (BdHN I), when the binary system has a sufficiently short distance and period, hypercritical accretion of SN ejecta onto the companion NS leads to the creation of a Kerr black hole (BH).

In this study, we focus on GRB 220101A, identified as a BdHN I[7]. The "inner engine" of BdHN I is a Kerr BH with mass M and angular momentum J, situated within an asymptotically uniform magnetic field B_0, aligned with the BH's rotation axis the Papapetrou-Wald solution[8,9]. This BH is surrounded by a rarefied plasma of ions and electrons[10]. The effective charge in the "inner engine", which is essential for explaining the 0.1-100 GeV radiation, arises from the gravitomagnetic interaction between the Kerr BH and the surrounding magnetic field[4,10–13]. Energy is extracted from the rotational energy of the Kerr BH, resulting in a decrease in its angular momentum. The 0.1-100 GeV emission is attributed to synchrotron radiation emitted by electrons and protons accelerated in an undercritical electric field regime see[10] for more details.

In Section 2, we present the observational details of GRB 220101A and provide a brief explanation of how we produced the corresponding 0.1-100 GeV luminosity. In Section 3, we describe the configuration of the electric field around the black hole. We also present the formulation of synchrotron radiation and the methodology for determining the mass and spin of the black hole. Finally, Section 4 offers the concluding remarks of the paper.

2. Observation of GRB 220101

GRB 220101A was sufficiently bright to trigger multiple satellites, including Swift[14,15], Fermi[16,17], AGILE[18], and Konus-Wind[19], with the trigger time recorded at 2022-01-01 05:11:13 (UT). The redshift of this gamma-ray burst (GRB) was determined to be $z = 4.61$[20,21]. Based on the observed data from Fermi/GBM and the known redshift, the equivalent isotropic energy is calculated to be $E_{\rm iso} = 4 \times 10^{54}$ erg[16,19].

For data in the GeV region, specifically in the 0.1-100 GeV range, we utilized the Large Area Telescope (LAT) onboard the Fermi satellite. The data were downloaded from the FSSC LAT Data server[a], and the flux was reproduced using the gtburst interface. Following the *Fermi* catalog guidelines[22], we performed a time-resolved likelihood spectral analysis by dividing the temporal data into logarithmically spaced bins. If the test statistic (TS) value of a bin was smaller than 20, we merged it with the subsequent bin and repeated the likelihood analysis. Over the total 1000 seconds of GeV emission observation, each statistically significant time bin was best fitted by a power-law spectrum. The total energy emitted in the 0.1-100 GeV range is $E_{\rm iso,GeV} = 2.93 \times 10^{53}$ erg, and its luminosity follows a power-law decay. See Figure 1 and Table 1 for detailed spectral analysis of each time bin and the overall behavior of its luminosity.

Start time (s)	End time (s)	Time-Error (s)	Alpha -	Luminosity (erg/s)	Luminosity Error (erg/s)
15.69	95	55.345	-2.65 ± 0.766	8.2×10^{50}	5.46×10^{50}
95	105	100	-4.78 ± 1.45	5.8×10^{51}	2.4×10^{51}
105	120	112.5	-3.82 ± 1.08	4.5×10^{51}	2.0×10^{51}
120	138	129	-2.56 ± 0.517	7.9×10^{51}	3.9×10^{51}
138	160	149	-2.06 ± 0.418	9.1×10^{51}	5.5×10^{51}
160	230	195	-1.67 ± 0.47	2.7×10^{51}	2.4×10^{51}
230	600	415	-2.08 ± 0.543	1.5×10^{51}	1.1×10^{51}
4200	6200	5200	-	1.8×10^{50}	-

[a] https://fermi.gsfc.nasa.gov/cgi-bin/ssc/LAT/LATDataQuery.cgi

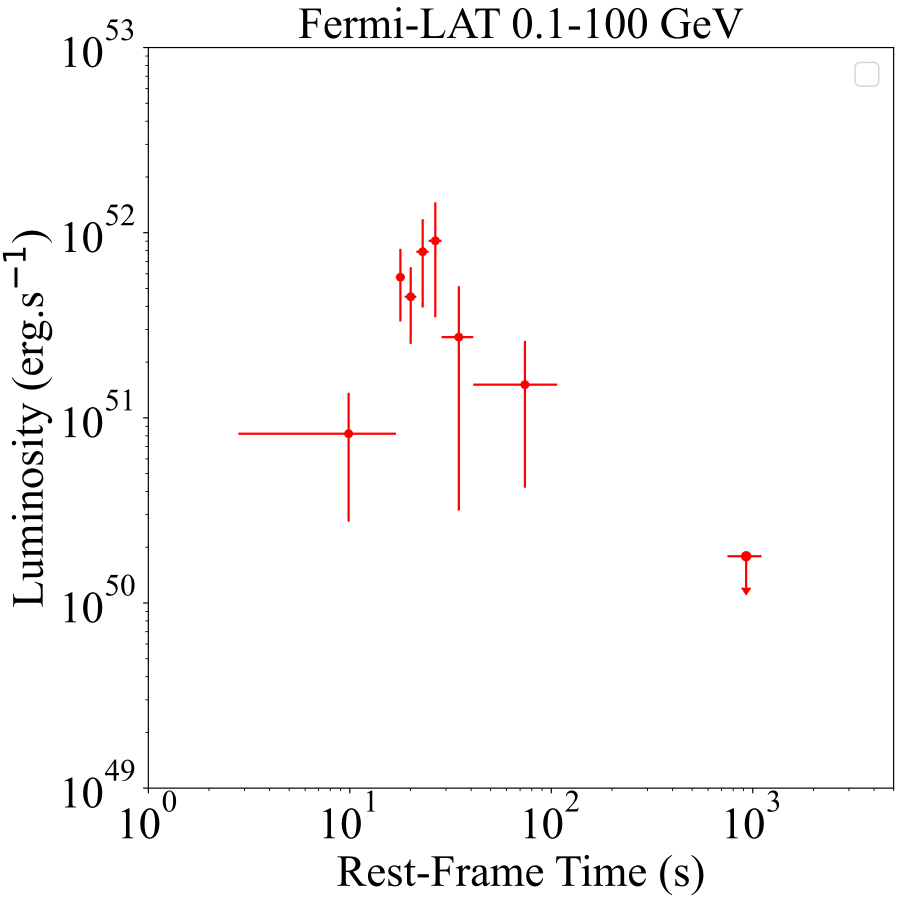

Fig. 1. 0.1-100 GeV luminosity of GRB 220101A obtained from Fermi-LAT.

3. Electric and Magnetic Fields Around Black Holes

The electromagnetic field in the polar direction $\theta = 0$ and at small angles from it is well approximated by[4,10]:

$$E_{\hat{r}} = -\frac{2B_0 J\,G}{c^3}\frac{\left(r^2 - \hat{a}^2\right)}{\left(r^2 + \hat{a}^2\right)^2}, \tag{1}$$

$$E_{\hat{\theta}} = 0, \tag{2}$$

$$B_{\hat{r}} = \frac{B_0\left(-\frac{4\,G\,J^2 r}{M(r^2+\hat{a}^2)} + a^2 + r^2\right)}{\left(r^2 + \hat{a}^2\right)}, \tag{3}$$

$$B_{\hat{\theta}} = 0. \tag{4}$$

The effective charge in the inner engine is defined as $Q_{\rm eff} = \frac{2B_0 J\,G}{c^3}$ 10. By substituting this effective charge into the charge of the Kerr-Newman solution, Eq. (1) matches the radial electric field of the Kerr-Newman metric in the same tetrad[23].

Therefore, up to linear order in θ and in the dimensionless BH spin parameter $\alpha \equiv \hat{a}/(GM/c^2)$, the electric field can be expressed as

$$E_{\hat{r}} \approx -\frac{2B_0 J\, G}{c^3}\frac{\left(r^2-\hat{a}^2\right)}{\left(r^2+\hat{a}^2\right)^2} \approx -\frac{1}{2}\alpha B_0 \frac{r_+^2}{r^2}. \tag{5}$$

where $r_+ = (\hat{M} + \sqrt{\hat{M}^2 - \hat{a}^2})$ is the (outer) event horizon, $\hat{M} = GM/c^2$, and $\hat{a} = a/c = J/(M\,c)$, being M and J the mass and angular momentum of the Kerr BH

3.1. *Acceleration in Non-Polar Axis*

For the current electric field, and assuming radial motion, the dynamics of electrons in the electromagnetic field, for $\gamma \gg 1$, is given by:

$$m_e c^2 \frac{d\gamma}{dt} = e\frac{1}{2}\alpha B_0 c - \frac{2}{3}e^4 \frac{B_0^2 \sin^2\langle\chi\rangle}{m_e^2 c^3}\gamma^2 \tag{6}$$

where where γ is the electron Lorentz factor, $\langle\chi\rangle$ is the injection angle between the direction of electron motion and the magnetic field, and m_r is the electron mass. For more detail see Ruffini et al., 2019[10].

The synchrotron spectrum peaks almost at the critical photon energy:

$$\epsilon_\gamma = \frac{3e\hbar}{2m_e c} B_0 \sin\langle\chi\rangle\,\gamma^2 = \frac{3}{2} m_e c^2 \beta \sin\langle\chi\rangle\,\gamma^2 \tag{7}$$

During the acceleration, the Lorentz factor increases linearly with time up to an asymptotic maximum value, which is set by the balance between the energy gain due to the acceleration in the electric field and the energy loss by the synchrotron radiation, equal to:

$$\gamma_{\rm max} = \frac{1}{2}\left(\frac{3}{e^2/(\hbar c)}\frac{\alpha}{\beta \sin^2\langle\chi\rangle}\right)^{\frac{1}{2}} \tag{8}$$

And the synchrotron cooling time scale $t = t_c$ for the maximum critical energy of photon is obtained as follows:

$$t_c = \frac{\hbar}{m_e c^2}\frac{3}{\sin\langle\chi\rangle}\left(\frac{e^2}{\hbar c}\alpha\beta^3\right)^{-\frac{1}{2}} \tag{9}$$

At the end of each process, all the available electromagnetic energy has been converted to the kinetic energy of the electron and the synchrotron radiation emitted in GeV band. The internal motor starts working again with the same magnetic field B_0, but with a new but slightly smaller angular momentum, $J = J_0 - \Delta J$ where ΔJ is the magnitude of the momentum extracted in the previous process.

So far, we know that the internal engine has three main parameters to measure, which are the mass of the black hole M, the spin of the black hole α, and the strength of the magnetic field around the black hole B_0. To obtain these three parameters, three physical and astrophysical conditions are needed. We also obtain the irreducible mass of the black hole, which is kept constant through the extraction process. The three main conditions are:

Condition 1:

First, we need the black hole spin energy to provide the energy budget for the observed GeV emission energy:

$$E_{\rm extra} \geq E_{\rm GeV} \tag{10}$$

According to the extractable energy formula and black hole mass[10,24–27], we reach the following inequality between M, α, and $E_{\rm GeV}$:

$$M \geq \frac{1}{\eta}\frac{E_{\rm GeV}}{c^2}, \quad \eta \equiv 1 - \sqrt{\frac{1+\sqrt{1-\alpha^2}}{2}} \tag{11}$$

We know that $\eta_{\rm max} \approx 0.293$ and $\alpha_{\rm max} = 1$. It is also important to remember that by keeping the irreducible mass constant in the energy extraction process, we are measuring a lower limit for the black hole mass. The irreducible mass increase means a higher mass for the black hole to account for the same GeV energy.

Condition 2:

A cloudy environment forms around this black hole and GeV photons need a transparent environment to escape from the electric and magnetic fields around the black hole. We will show here the necessary transparency for photons to escape. The attenuation coefficient for this process is equal to:

$$\beta \ll \frac{16}{9}\frac{e^2}{\hbar c}\frac{1}{\alpha} \approx \frac{1.298\times 10^{-2}}{\alpha}, \quad B_0 \ll \frac{5.728\times 10^{11}}{\alpha}\,\mathrm{G} \tag{12}$$

$$\overline{R} \approx 0.23\frac{e^2}{\hbar c}\left(\frac{\hbar^2}{m_e c}\right)^1 \beta \sin\langle\chi\rangle \exp\left(-\frac{4/3}{\psi}\right) \tag{13}$$

Condition 3:

The duration of synchrotron radiation or cooling time t_c obtained from the previous equations should be equal to the observed duration of GeV emission:

$$\tau_{\rm rad,1} = \frac{\mathcal{E}_1}{L_{\rm GeV,1}} \tag{14}$$

where $\mathcal{E}$ is the electrostatic energy available for the process. The subscript "1" refers to values evaluated at the beginning of the GeV emission transparency (i.e., at the end of the UPE phase) at $t = t_{\rm rf,UPE}$. Therefore, the third equation of the system is:

$$t_c\left(\langle\chi\rangle, \alpha, \beta\right) = \tau_{\rm rad,1}\left(\mu, \alpha, \beta, L_{\rm GeV,1}\right) \tag{15}$$

Therefore, by applying these three conditions, the three main parameters of the internal engine are defined as follows:

We insert and apply the (1-21) to obtain a lower limit for the mass and spin of the black hole.

By inserting the (1-29) of the second condition for a certain α, we get the upper limit of the magnetic field.

We obtain the following expression for β as a function of α, observable luminosity and energy, $E_{\rm GeV}$ and $L_{\rm GeV}$ respectively:

$$\beta\left(\epsilon_\gamma, E_{\rm GeV}, L_{\rm GeV,1}, \alpha\right) = \frac{1}{\alpha}\left(\frac{64}{9}\sqrt{3\frac{e^2}{\hbar c}}\frac{\epsilon_\gamma}{B_c^2 r_+\left(\mu,\alpha\right)^3}\frac{L_{\rm GeV,1}}{eB_c c^2}\right)^{2/7} \tag{16}$$

Using the values obtained in Section 2, namely $\mathrm{E_{GeV}} = 2.93 \times 10^{53}\,\mathrm{erg}$ and a peak luminosity of $\mathrm{L_{GeV}} = 9.1 \times 10^{51}\,\mathrm{erg\,s^{-1}}$, the final values are: $\beta = 6.8 \times 10^{-4}$, $\alpha = 0.546$, $M = 3.94\,\mathrm{M_\odot}$, and $M_{\rm irr} = 3.78\,\mathrm{M_\odot}$, which are well aligned with typical black holes previously observed in GRBs.

4. conclusions

In conclusion, our analysis of GRB 220101A demonstrates the viability of the Binary Driven Hypernova model in explaining the observed GeV emission attributed to a newborn Kerr black hole. By meticulously analyzing the data obtained from the Fermi/LAT observations, we have established a compelling correlation between the characteristics of the emission and the fundamental properties of the black hole, including its mass and spin. The findings align with theoretical predictions, reinforcing the notion that such gamma-ray bursts are closely linked to the dynamics of newly formed black holes.

Moreover, the determination of the black hole's mass at approximately 3.94 solar masses and its spin parameter of 0.546 further underscores the complex interplay between gravitational dynamics and electromagnetic processes in extreme astrophysical environments. This work not only enriches our understanding of GRB mechanisms but also paves the way for future investigations into the role of black holes in cosmic events. We acknowledge that the synchrotron radiation presented here may need to be replaced by curvature radiation, and that the transparency condition requires further detailed consideration, which will be the focus of future works.

References

1. R. Ruffini, M. Karlica, N. Sahakyan, J. A. Rueda, Y. Wang, G. J. Mathews, C. L. Bianco and M. Muccino, A GRB Afterglow Model Consistent with Hypernova Observations, **869**, p. 101 (December 2018).
2. Y. Wang, J. A. Rueda, R. Ruffini, L. Becerra, C. Bianco, L. Becerra, L. Li and M. Karlica, Two Predictions of Supernova: GRB 130427A/SN 2013cq and GRB 180728A/SN 2018fip, **874**, p. 39 (March 2019).
3. J. A. Rueda, R. Ruffini, M. Karlica, R. Moradi and Y. Wang, Magnetic Fields and Afterglows of BdHNe: Inferences from GRB 130427A, GRB 160509A, GRB 160625B, GRB 180728A, and GRB 190114C, **893**, p. 148 (April 2020).
4. J. A. Rueda and R. Ruffini, The blackholic quantum, *European Physical Journal C* **80**, p. 300 (April 2020).
5. R. Ruffini, R. Moradi, J. A. Rueda, L. Li, N. Sahakyan, Y. C. Chen, Y. Wang, Y. Aimuratov, L. Becerra, C. L. Bianco, C. Cherubini, S. Filippi, M. Karlica, G. J. Mathews, M. Muccino, G. B. Pisani and S. S. Xue, The morphology of the X-ray afterglows and of the jetted GeV emission in long GRBs, *MNRAS* (March 2021).
6. G. B. Pisani, R. Ruffini, Y. Aimuratov, C. L. Bianco, M. Kovacevic, R. Moradi, M. Muccino, A. V. Penacchioni, J. A. Rueda, S. Shakeri and Y. Wang, On the Universal Late X-Ray Emission of Binary-driven Hypernovae and Its Possible Collimation, **833**, p. 159 (December 2016).
7. C. L. Bianco, M. T. Mirtorabi, R. Moradi, F. Rastegarnia, J. A. Rueda, R. Ruffini, Y. Wang, M. Della Valle, L. Li and S. R. Zhang, Probing Electromagnetic Gravitational-wave Emission Coincidence in a Type I Binary-driven Hypernova Family of Long Gamma-Ray Bursts at Very High Redshift, **966**, p. 219 (May 2024).
8. A. Papapetrou, Champs gravitationelle stationaires a symetrie axiale, *Annales de L'Institut Henri Poincare Section (A) Physique Theorique* **4**, p. 83 (December 1966).
9. R. M. Wald, Black hole in a uniform magnetic field, **10**, 1680 (September 1974).
10. R. Ruffini, R. Moradi, J. A. Rueda, L. Becerra, C. L. Bianco, C. Cherubini, S. Filippi, Y. C. Chen, M. Karlica, N. Sahakyan, Y. Wang and S. S. Xue, On the GeV Emission of the Type I BdHN GRB 130427A, **886**, p. 82 (Dec 2019).
11. R. Moradi, J. A. Rueda, R. Ruffini and Y. Wang, The newborn black hole in GRB 191014C proves that it is alive, **649**, p. A75 (May 2021).
12. R. Moradi, J. A. Rueda, R. Ruffini, L. Li, C. L. Bianco, S. Campion, C. Cherubini, S. Filippi, Y. Wang and S. S. Xue, Nature of the ultrarelativistic prompt emission phase of GRB 190114C, **104**, p. 063043 (September 2021).
13. F. Rastegarnia, R. Moradi, J. A. Rueda, R. Ruffini, L. Li, S. Eslamzadeh, Y. Wang and S. S. Xue, The structure of the ultrarelativistic prompt emission phase and the properties of the black hole in GRB 180720B, *European Physical Journal C* **82**, p. 778 (September 2022).
14. A. Tohuvavohu, J. D. Gropp, J. A. Kennea, A. Y. Lien, D. M. Palmer, T. M. Parsotan, B. Sbarufatti, M. H. Siegel and Neil Gehrels Swift Observatory Team, GRB 220101A: Swift detection of a burst with a bright optical counterpart, *GRB Coordinates Network* **31347**, p. 1 (January 2022).
15. A. Tohuvavohu, GRB 220101A: Correction to GCN 31347, *GRB Coordinates Network* **31348**, p. 1 (January 2022).
16. S. Lesage, C. Meegan and Fermi Gamma-ray Burst Monitor Team, GRB 220101A: Fermi GBM Detection, *GRB Coordinates Network* **31360**, p. 1 (January 2022).
17. M. Arimoto, L. Scotton, F. Longo and Fermi-LAT Collaboration, GRB 220101A: Fermi-LAT detection, *GRB Coordinates Network* **31350**, p. 1 (January 2022).
18. A. Ursi, E. Menegoni, F. Longo, C. Pittori, F. Verrecchia, P. Tempesta, M. Tavani,

A. Argan, M. Cardillo, C. Casentini, Y. Evangelista, L. Foffano, G. Piano, F. Lucarelli, A. Bulgarelli, A. di Piano, V. Fioretti, F. Fuschino, N. Parmiggiani, M. Marisaldi, M. Pilia, A. Trois, I. Donnarumma, A. Giuliani and Agile Team, GRB 220101A: AGILE detection, *GRB Coordinates Network* **31354**, p. 1 (January 2022).

19. A. Tsvetkova, D. Frederiks, A. Lysenko, A. Ridnaia, D. Svinkin, M. Ulanov, T. Cline and Konus-Wind Team, Konus-Wind detection of GRB 220101A, *GRB Coordinates Network* **31433**, p. 1 (January 2022).
20. D. A. Perley, GRB 220101A: Liverpool telescope imaging of a high-redshift afterglow, *GRB Coordinates Network* **31357**, p. 1 (January 2022).
21. J. P. U. Fynbo, A. de Ugarte Postigo, D. Xu, D. B. Malesani, B. Milvang-Jensen and J. Viuho, GRB 220101A: NOT redshift confirmation, *GRB Coordinates Network* **31359**, p. 1 (January 2022).
22. Ackermann et al., The First Fermi-LAT Gamma-Ray Burst Catalog, **209**, p. 11 (November 2013).
23. R. Giacconi and R. Ruffini (eds.), *Physics and astrophysics of neutron stars and black holes* 1978.
24. D. Christodoulou, Reversible and Irreversible Transformations in Black-Hole Physics, *Physical Review Letters* **25**, 1596 (November 1970).
25. D. Christodoulou and R. Ruffini, Reversible Transformations of a Charged Black Hole, **4**, 3552 (December 1971).
26. S. W. Hawking, Gravitational Radiation from Colliding Black Holes, *Physical Review Letters* **26**, 1344 (May 1971).
27. C. W. Misner, K. S. Thorne and J. A. Wheeler, *Gravitation* (Freeman and Co., San Francisco, 1973).